ELSEVIER

Journal of Structural Geology 29 (2007) 1002–1021

JOURNAL OF STRUCTURAL GEOLOGY

www.elsevier.com/locate/jsg

Orthorhombic fault–fracture patterns and non-plane strain in a synthetic transfer zone during rifting: Lennard shelf, Canning basin, Western Australia

John McL. Miller [a,*,1], E.P. Nelson [b], M. Hitzman [b], P. Muccilli [c], W.D.M. Hall [d]

[a] *Australian Crustal Research Centre, School of Geosciences, Monash University 3168, Australia*
[b] *Department of Geology and Geological Engineering, Colorado School of Mines, Golden, CO 80401, USA*
[c] *Mincor Resources NL, PO Box 1810, West Perth, WA 6872, Australia*
[d] *School of Geosciences, Monash University 3168, Australia*

Received 19 June 2006; received in revised form 9 January 2007; accepted 17 January 2007
Available online 7 February 2007

Abstract

A complex series of faults occur within transfer zones normal to the WNW-trending rifted northern margin of the Canning basin (Western Australia). These zones controlled basinal fluid flow and the formation of some carbonate-hosted Mississippi Valley-type Zn–Pb deposits along the basin margin during Devonian to Carboniferous rifting. The study area has a regional fault geometry similar to a synthetic overlapping transfer zone. Surface and underground mapping in this transfer zone, combined with 3D modelling, indicate the faults and related extension fractures have an orthorhombic geometry. The orthorhombic fault–fracture mesh developed in response to three-dimensional non-plane strain in which the intermediate finite extension magnitude was non-zero. Pre-mineralisation marine calcite fill in the fault–fracture mesh indicates that it formed early in the deformation history. Later deformation that overprints the Zn–Pb mineralisation and fault–fracture mesh, was associated with a different maximum extension direction and this modified and reactivated the faults with both dip-slip and oblique-slip movement and tilting of earlier structures. The orthorhombic geometry is not observed at a regional scale ($>10 \times 10$ km), indicating probable scale-dependant behaviour. This study indicates that this transfer zone developed either by (1) strain partitioning with synchronous strike-slip structures and adjacent zones of non-plane extension, or (2) by a component of non-plane extension sub-parallel to the basin margin followed by subsequent transtensional overprint of the system (preferred model). Synthetic overlapping transfer zones are inferred to be key regions where orthorhombic fault geometries may develop.

Keywords: Basin evolution; Rift; Normal fault; Transfer zone; MVT deposit

1. Introduction

The geometry of rift systems formed by continental extension has a major control on the location of petroleum and mineral deposits, on the architecture of associated sedimentary sequences, and also on the position of oceanic fracture zones that form during later ocean spreading (e.g., Lister et al., 1991; Guiraud and Martin, 1992; Miller et al., 2002). Many rift systems are segmented and display along-strike offsets in depocenters and/or changes in extensional fault polarities. There is some conflicting terminology in the literature, however, and two end-member geometric models have been proposed to account for changes in fault polarities and offset depocenters (McClay et al., 2002): (1) the hard-linked strike-slip or oblique-slip transfer fault model (e.g., Bally, 1981; Gibbs, 1983, 1984; Lister et al., 1986) and (2) the soft-linked accommodation zone model of distributed faulting

* Corresponding author. Tel.: +61 8 64885803.
E-mail address: jmmiller@cyllene.uwa.edu.au (J.McL. Miller).
[1] Now at Centre for Exploration Targeting, School of Earth and Geographical Sciences, University of Western Australia 6009, Australia.

0191-8141/$ - see front matter © 2007 Elsevier Ltd. All rights reserved.
doi:10.1016/j.jsg.2007.01.004

without distinct cross faults or transfer faults (e.g., Bosworth, 1985; Rosendahl et al., 1986; Walsh and Watterson, 1991; Morley et al., 1990; Morley, 1994; Moustafa, 1997; Faulds and Varga, 1998). The term transfer zone has previously been used as a broad definition that covers both soft and hard-linked geometries, and this includes relay-ramps between two normal faults that over step in map view and have the same dip direction (e.g., Morley et al., 1990). Morley et al. (1990) defines a synthetic transfer zone as a region where displacement transfer occurs between faults with the same dip direction, and a conjugate transfer zone where the main normal faults dip in opposite directions.

Within the Canning basin of Western Australia (Fig. 1) faults at right angles to the basin margin offset depocenters and have had a major control on basinal fluid flow and the formation of structurally-controlled Mississippi Valley-type Pb–Zn deposits (e.g., Vearncombe et al., 1995). These faults have been inferred to represent transtensional zones, and have been referred to as either transfer zones with both normal and strike-slip faults (Vearncombe et al., 1995) or as transtensional accommodation zones (Dörling et al., 1996a,b). In this contribution we have used the terminology of Morley et al. (1990) and Peacock et al. (2000), and define these regions as transfer zones. The Canning basin has undergone almost no inversion, and its northern margin has excellent surface exposures, underground mines on key fault segments, seismic and drill data from petroleum exploration that have been previously utilised to produce high quality structural maps (e.g., Fig. 4 of Dörling et al., 1996a). These features make the Lennard shelf of the Canning basin (Fig. 1) an excellent area to study the mechanics of basin formation.

This paper incorporates earlier regional and mine-based studies (McManus and Wallace, 1992; Vearncombe et al., 1995; Dörling et al., 1996a,b; Playford and Wallace, 2001; Wallace et al., 2002) with new information on the basement architecture and data from the Pillara Pb–Zn mine situated on one of the major transfer zones on the Lennard shelf. The transfer zone studied has a regional geometry consistent with being a synthetic overlapping transfer zone (Morley et al., 1990), and has developed in an area between two over stepping normal faults with the same dip direction (Figs. 1c, 2a).

The paper documents the structural history within the transfer zone, which is used as an additional constraint to improve our understanding of basin formation. We argue that field relations within the transfer zone are more consistent with it being a dominantly extensional structure with non-plane strain in which the intermediate finite elongation magnitude is non-zero. This zone represents a transfer zone that was associated with a component of extension orthogonal to the regional maximum finite elongation direction. Furthermore, the mapped fault and fracture geometries within the transfer zone have a 2D rhombic map pattern, and do not conform to widely accepted Andersonian (Anderson, 1951) models of fault development (Fig. 2b). Instead they are inferred to have orthorhombic geometry (Fig. 2c; Oertel, 1965; Aydin and Reches, 1982; Reches and Dietrich, 1983), and define the fault system within this particular synthetic overlapping transfer zone. Orthorhombic is a symmetry system with three mutually perpendicular axes of different length. Here, and in the literature cited, orthorhombic is used to refer to fault geometry, with the implication that this geometry reflects a strain field in which the lengths of the principal strain axes are non-equal. Reviews of Mohr–Coloumb and orthorhombic fault models argue that the current experimental and field data provide no clear evidence in favour of either model (e.g., Mandl, 2000, p. 155). Identification of orthorhombic fault systems within large fault-controlled basins is commonly complicated by multiple extension events, extension directions that change through time, complex basement rheology, and later basin inversion.

2. Geological framework

2.1. Canning basin and Lennard shelf

The Canning basin is a major intracratonic basin within the Australian craton (Fig. 1a, b). The basin is bounded to the south by the Archaean Pilbara craton and to the north by the Proterozoic Kimberley block (Fig. 1a). Intracratonic downwarping during the Early Ordovician resulted in the deposition of shallow marine sandstone and carbonate rock (Brown et al., 1984). Extension during the Middle Devonian to early Carboniferous led to the development of the WNW-trending Fitzroy trough with up to 15 km of Paleozoic strata along the northeastern margin of the basin. These strata are characterised by basin margin reef complexes and basinal carbonate and siliciclastic turbidites (Playford, 1980; George et al., 1997).

The northeastern side of the Canning basin is bounded by the Lennard shelf (Fig. 1b). The distribution of Devonian lithofacies on the Lennard shelf was controlled by movement on basement blocks, with reef and platform facies confined to paleo-highs and basin facies in adjacent areas. In the latest Devonian the reef complexes were drowned and conformably covered by early Carboniferous shallow marine units. In the Late Triassic regional dextral wrench faulting affected the central region of the Fitzroy trough (Middleton, 1990).

The Emmanuel and Pillara Ranges (Fig. 1c) expose a 50 km portion of the Lennard shelf, and contain faults that are parallel and perpendicular to the margin of the Canning basin. The Pinnacle fault zone separates the Lennard shelf from the Fitzroy trough, and the Virgin Hills fault zone is sub-parallel and northeast of the Pinnacle fault (Fig. 1c).

NNE-trending structures are prominent features of the Lennard shelf (Fig. 1c) and previously have been interpreted as transtensional zones that developed synchronously with extensional pull-apart basins (e.g., Vearncombe et al., 1995). The Albatross fault is one of these structures, and a number of NNE-trending faults occur west of the Albatross fault (Fig. 1c). These faults control the trend of the Limestone Billy Hills (Fig. 3), which is the only NNE-trending range along the Lennard shelf (the Oscar, Pillara and Emmanuel ranges all trend WNW; Fig. 1c). We define this NNE-trending set of faults zone as the Limestone Billy Hills Transfer Zone (LBHTZ; Fig. 1c).

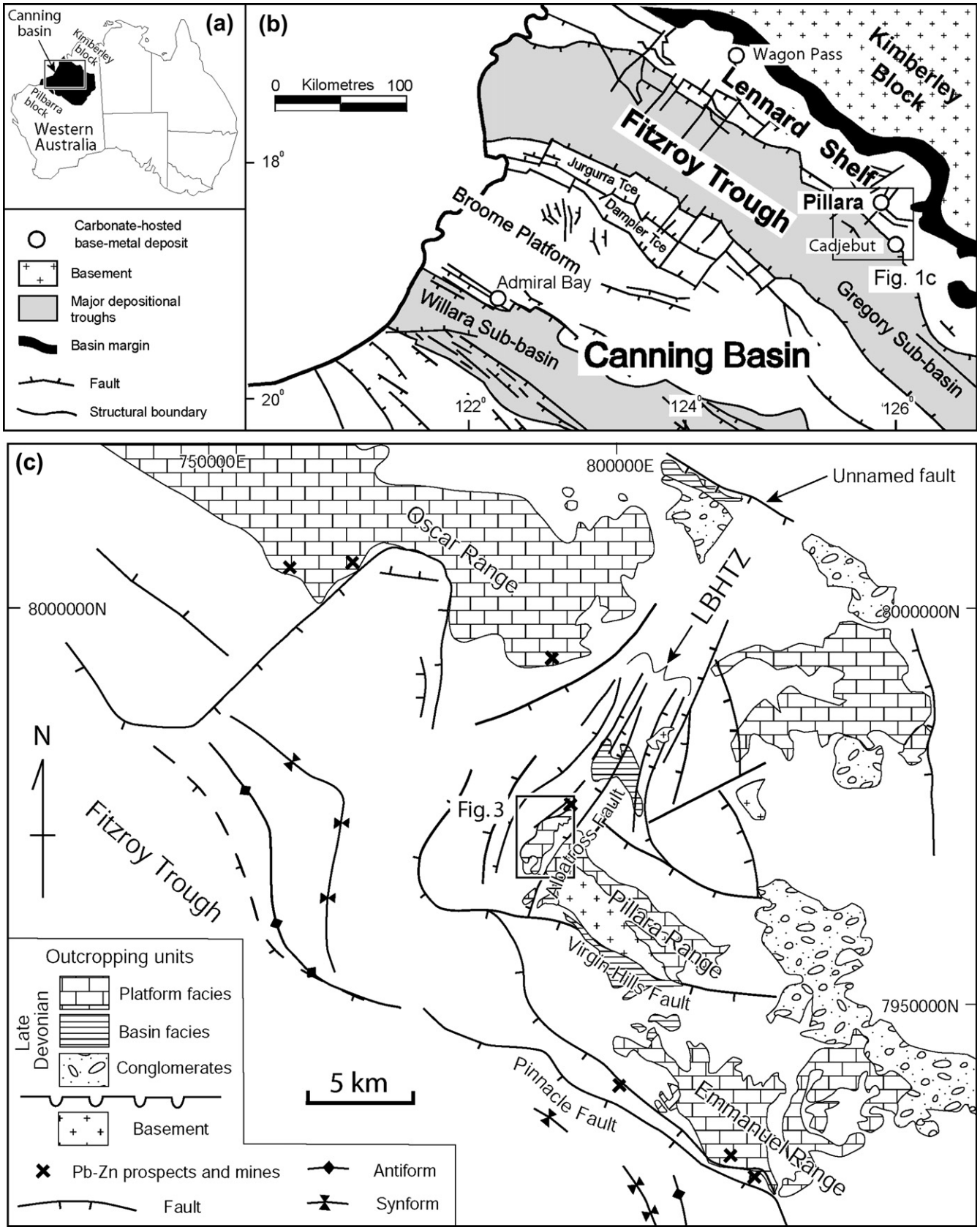

Fig. 1. (a) Location map of the Canning basin. (b) Geological map of the Canning basin. Rectangle shows location of Fig. 1c. (c) Geological map of a portion of the Lennard shelf (after Dörling et al., 1996b). Limestone Billy Hills Transfer Zone is annotated as LBHTZ.

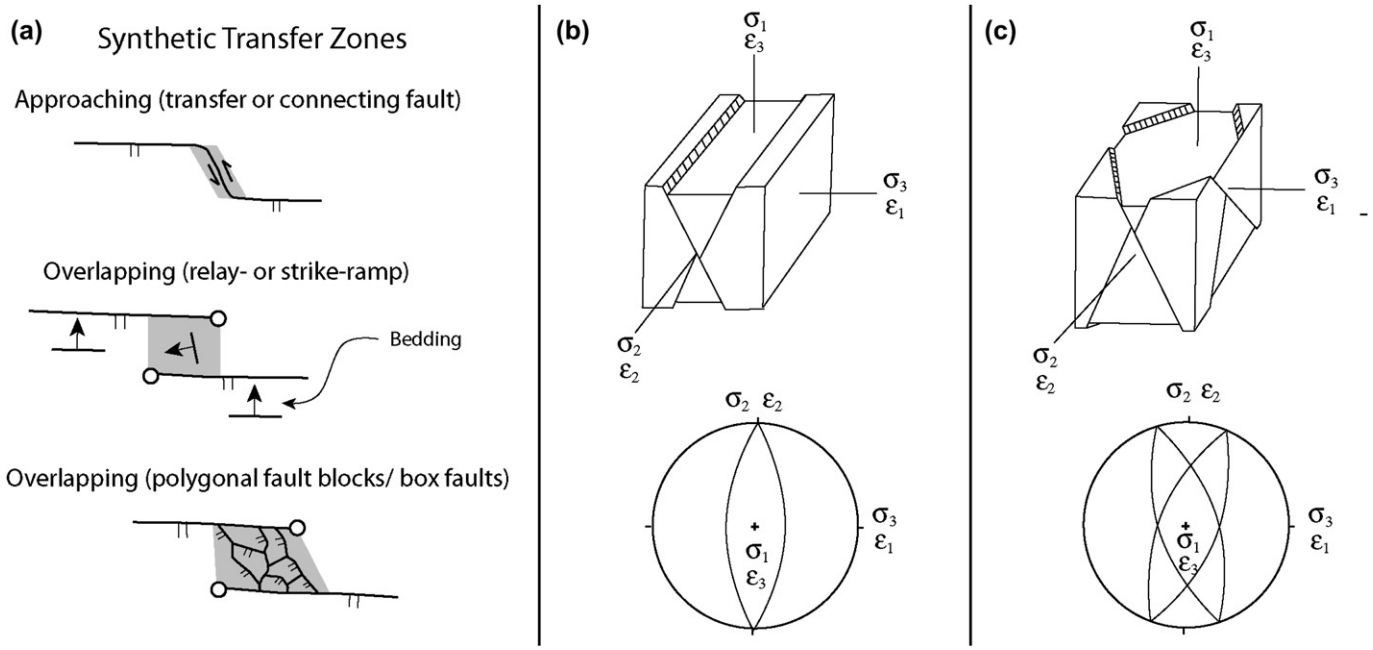

Fig. 2. Schematic maps of fault models showing relationship of synthetic transfer zones (from Morley et al., 1990) and block diagrams and stereone to showing principal stresses (σ_1, σ_2, σ_3), and principal finite extensions (ϵ_1, ϵ_2, ϵ_3) (modified from Reches, 1983). (a) Types of synthetic transfer zones as defined by Morley et al. (1990). Overlapping transfer zones can be either relay- or strike-ramps where a dip variation in bedding conserves regional extensional strain between two normal faults. Alternatively, this can be achieved with a series of faults. In many areas an overlapping transfer zone will start as a relay- or strike-ramp and then subsequently become breached by faults that connect between the two synthetic normal faults (e.g., Childs et al., 1995). Grey areas highlight the transfer zone. (b) Conjugate normal fault geometry associated with plane strain predicted by Andersonian fault theory (Anderson, 1951). (c) Orthorhombic fault geometry associated with non-plane strain (Reches, 1978, 1983; Reches and Dietrich, 1983; Krantz, 1988a,b).

At the regional scale, the NNE-trending faults within the LBHTZ have developed in an area that is between two over stepping faults (Virgin Hills fault and highlighted unnamed fault at northeastern section of Fig. 1c). The current regional structural models interpret that the Albatross fault terminates against the Virgin Hills fault (Fig. 3), a geometry not indicative of a major strike-slip transfer fault. Furthermore, the basin bounding Pinnacle fault has been projected to another basin bounding fault to the northwest (note dashed line on Fig. 1c). There is no change in half graben polarity, nor is there evidence for a major step in the overall basin margin along strike (Fig. 1c) across the LBHTZ. The LBHTZ developed in an area between two over stepping normal faults with the same dip direction (Fig. 1c), and is therefore similar to a breached relay- or strike-ramp (Morley et al., 1990; Childs et al., 1995; Peacock et al., 2000). The LBHTZ has a regional geometry most consistent with being termed a synthetic overlapping transfer zone dominated by numerous complex fault blocks instead of being a simple relay- or strike-ramp (Fig. 2a; Morley et al., 1990).

The Emmanuel Range, and Limestone Billy Hills region, are host to a number of Mississippi Valley-type (MVT) Zn–Pb deposits which are notable for their strong structural control (Fig. 1c; Murphy, 1990; Vearncombe et al., 1995, 1996; Dörling et al., 1996a,b). These deposits are carbonate-hosted sulfide deposits consisting of sphalerite, galena, and iron sulfides in various stratabound bodies, replacement bodies, and fault-controlled vein and breccia bodies with open-space fill. Carbonate cement relationships (McManus and Wallace, 1992) combined with Rb–Sr dating of sphalerite and U–Pb dating of ore stage calcite (Christensen et al., 1995; Brannon et al., 1996) constrain mineralisation to have occurred during or within 10 million years of early burial diagenesis in the Late Devonian to earliest Carboniferous (350 ± 15 Ma). The MVT deposits developed by infiltration of metalliferous basinal brines derived from basin compaction and dewatering during the final stages of Late Devonian to Early Carboniferous extension (e.g., Wallace et al., 2002).

2.2. Limestone Billy Hills region

The Limestone Billy Hills region exposes predominantly N-dipping Givetian–Frasnian platform carbonates with a narrow fringe of reef-margin and fore-reef units along the western and northern sides of the block (Fig. 3). The southern Limestone Billy Hills region exposes the lowest stratigraphic units as well as the underlying massive basement granitoids (Fig. 3). The carbonate units are disrupted by a series of predominantly NE- and N-trending normal faults that control the trend of the Limestone Billy Hills and have a rhombic pattern in plan view (Figs. 3, 4). These faults have both east and west dips, producing a series of small horsts and grabens. Many of the faults have abrupt strike changes and in places have dip reversals along strike (Fig. 3).

Fault–vein relationships immediately to the east of the Limestone Billy Hills area have been used to infer a component of

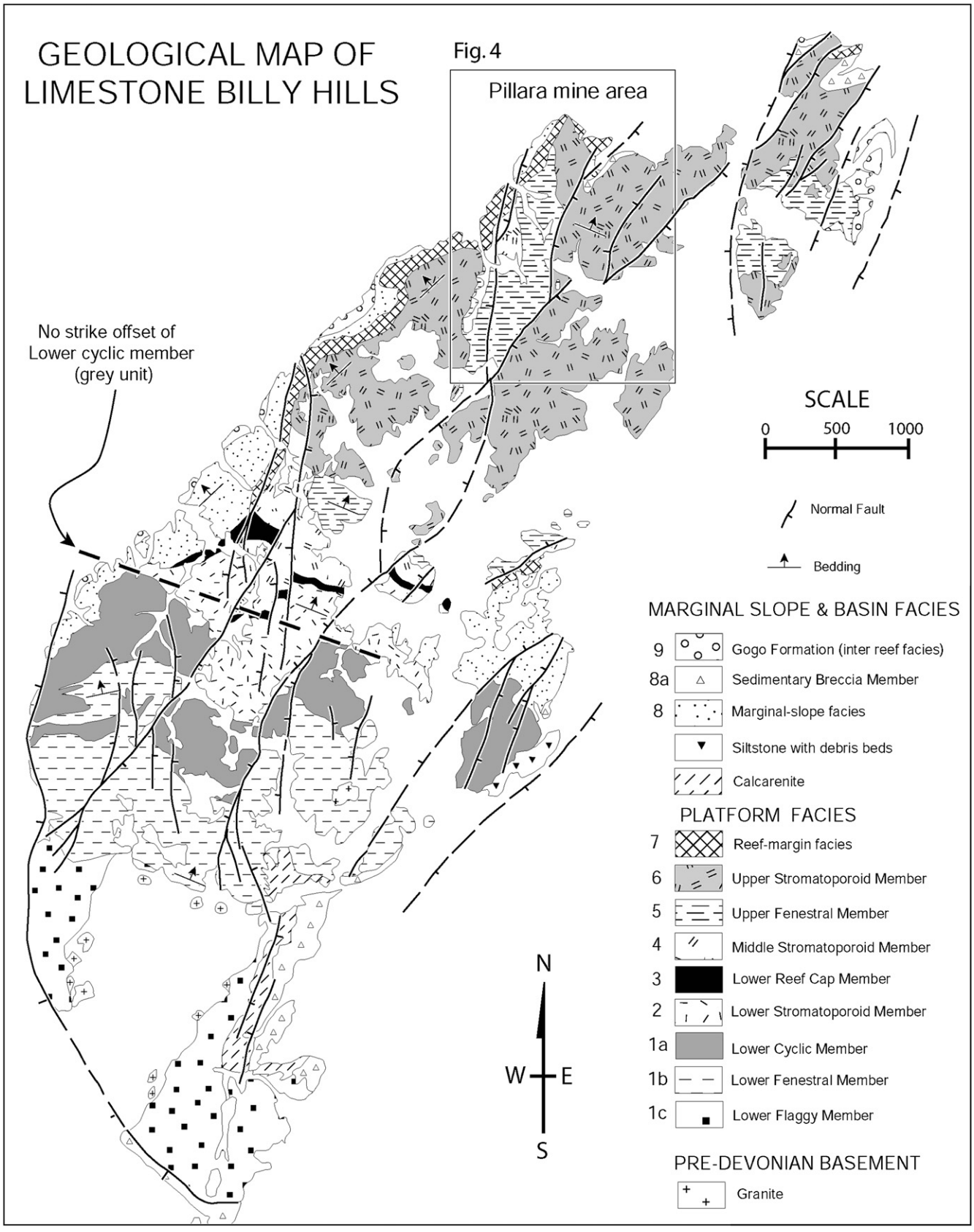

Fig. 3. Geological map of the Limestone Billy Hills area (after Hall, 1984); location shown on Fig. 1c. Location of Fig. 4 is shown.

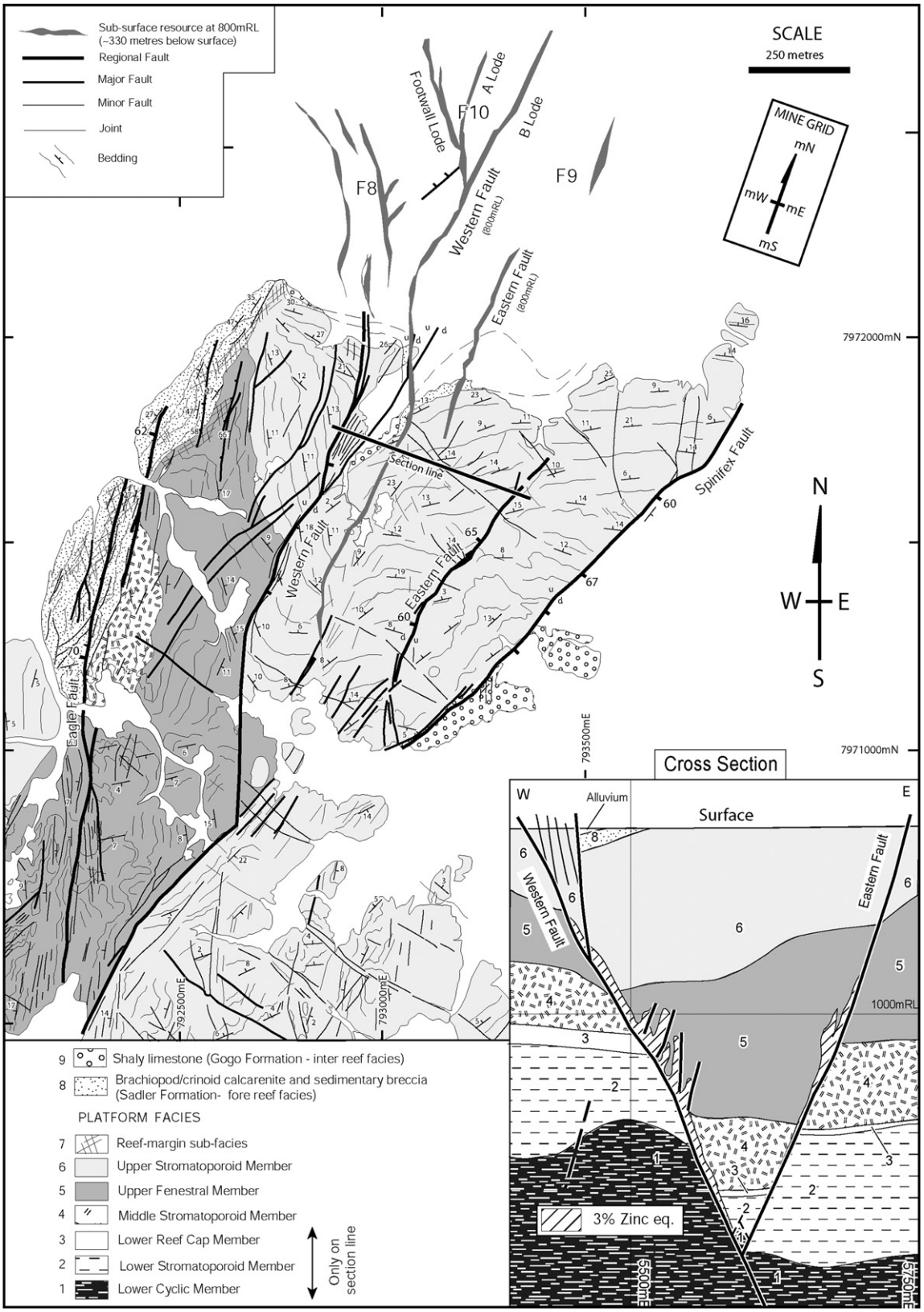

Fig. 4. Geological map of the Pilllara mine area, northern Limestone Billy Hills; location shown on Fig. 3. Subsurface resource is highlighted with grey outlines. F8, F9, and F10 are areas within the mine. Section line for cross section inset is marked. (Inset) Geological profile of Western and Eastern faults. Numbers represent the stratigraphic units defined in the key. Note the differential thickness of unit 5 in the hangingwall and footwall of both the Western and Eastern faults. This provides evidence that growth faulting occurred. The geometry at the intersection between the Eastern and Western fault is poorly constrained by available data. Diagonal lined pattern represents the 3% zinc equivalence cut off. Zinc equivalence is a conversion that changes the lead weight percent to an equivalent zinc percent (based on the metal price at the time); this value is added to the actual zinc percent.

sinistral strike-slip movement along the Albatross fault zone (Dörling et al., 1996a,b). However, within the Limestone Billy Hills area there is no consistent strike separation of stratigraphic units across the main NE-striking graben (thick dashed line in Fig. 3), suggesting no significant strike-slip movement (Fig. 3). Rather, normal faulting of shallowly north-dipping strata produces both dextral and sinistral separation in plan view (Fig. 3).

3. Pillara Zn–Pb deposit

3.1. Main structural features

The Pillara deposit (formerly termed Blendevale, e.g., Vearncombe et al., 1995) occurs within a graben at the northern end of the Limestone Billy Hills (Fig. 4). The graben is defined by the Western and Eastern faults that, in profile, have a conjugate geometry (cross section in Fig. 4) (Vearncombe et al., 1995). The strata in the hangingwall of these faults preserve evidence for growth faulting indicating that faulting began early during sedimentation (note thickness changes within unit 5 in Fig. 4). The faults in the direct vicinity of the orebody have variable strikes (Fig. 5) with north and northeast strikes dominant, and abrupt changes in strike producing rhombic map patterns (Figs. 4, 5). The majority of ore consists of sulfide-matrix breccia associated with these faults (Fig. 6a, b and c); polyphase breccia is common. Fault dip refracts through different stratigraphic units producing narrow, high-grade ore zones where the faults dilate on steep sections.

Colloform sulfide textures indicate that mineralisation occurred mainly by open space filling along faults (Fig. 6b), although replacement textures also exist. Sub-vertical extension veins with Zn–Pb sulfides occur in the footwall and hangingwall of the faults (Figs. 6d, e, 7 and 8) and show the same mineral paragenesis as the fault breccias. The extension veins show strike variations similar to that of the faults (Fig. 5), and commonly form a rhombic pattern in map view (Fig. 8). Whilst we have termed these extension veins, there are few stratigraphic markers across these structures, and in some areas the veins are hybrid, or extensional shear veins.

The vein fill varies between deeper and shallower structural levels (deeper levels are areas where units 1 and 2 define the hangingwall stratigraphy; shallower levels are where unit 6 defines the hangingwall stratigraphy). The primary paragenetic sequence in veins at shallow structural levels is marine calcite, marcasite, sphalerite–galena followed by sparry calcite (Fig. 7a, b). In some areas there are multiple generations of sphalerite. At deeper structural levels the initial fill is normally marcasite (Fig. 7c, d), but in most cases the major faults still have early laminated marine calcite (Fig. 6c). These early calcite veins are commonly referred to as Neptunian dykes. Late-stage faulting and mineralisation formed breccias with clasts preserving earlier sulfide minerals and veins dominated by galena and calcite gangue.

Compared to the Eastern fault the Western fault is laterally more extensive and is more complex, with multiple mineralised and non-mineralised faults splaying from it (Fig. 5). The non-mineralised faults contain early marine carbonate cement and marcasite-calcite cemented breccia (e.g., the northeast-striking Franklin fault; Fig. 5), but contain no ore stage sulfides, and are truncated by late-stage syn-ore movement along the Western fault.

In some areas, late-stage faults crosscut the earlier mineralised breccias, veins and faults (Fig. 9). These faults are associated with breccias that have a predominantly calcite matrix and vertical extension veins that contain galena and calcite. Unlike the earlier generations of extension veins, these have a relatively consistent opening direction (Fig. 9d, large net).

3.2. Slip vector orientation

The orientations of extension veins in the direct hangingwall and footwall of faults are commonly used to determine the orientation of the fault slip vector (e.g., Robert and Poulsen, 2001; Miller and Wilson, 2004). The slip vector orientation on a fault is inferred to be perpendicular to the intersection of the fault with the footwall or hangingwall extension veins. In addition, shear sense of the strike-slip component can be inferred from the strike relationship between extension veins and the fault they are associated with (e.g., veins striking clockwise from a fault imply dextral movement). However, application of this methodology to the Pillara Zn–Pb deposit is complicated by the strike variability of the steep extension and extensional shear veins. This reflects the scale problems associated with mapping underground drives, and with structural analysis of individual outcrops. In order to visualise the extension vein and fault geometries at a larger scale, a three-dimensional model of the Pillara mine was built. This model was constructed by digitising two-dimensional vertical cross sections at 25 m intervals and using these sections to produce a three-dimensional wire frame of the stratigraphic contacts and faults. The positions of stratigraphic contacts were verified with the positions determined from the two-dimensional cross sections constructed from diamond drill hole data. The most reliable areas of the model are directly adjacent to the faults where greater drilling density exists. As mineralisation was strongly controlled by structure, a 3% zinc equivalent grade cut-off was used to model the orebodies formed along major faults and extension veins. Extension veins and faults were distinguished by checking for stratigraphic offsets across the mineralised zones.

The kinematics of the Eastern and Western faults were analysed by assuming that the slip vector in the fault plane is perpendicular to the intersection of extension veins with the fault plane. The three-dimensional model clearly shows extension veins in the direct hangingwall of the Eastern fault (these do not offset stratigraphy; Fig. 10a, b). The lines of intersection of these veins with the fault have a horizontal or slightly north-plunging rake ($<10^\circ$) in the fault plane (dashed lines on Fig. 10a), indicating this was probably a pure dip-slip fault during mineralisation. These intersection lines are not parallel to cut-off lines of stratigraphic contacts in the footwall or hangingwall of the fault (Fig. 10c), showing that the veins

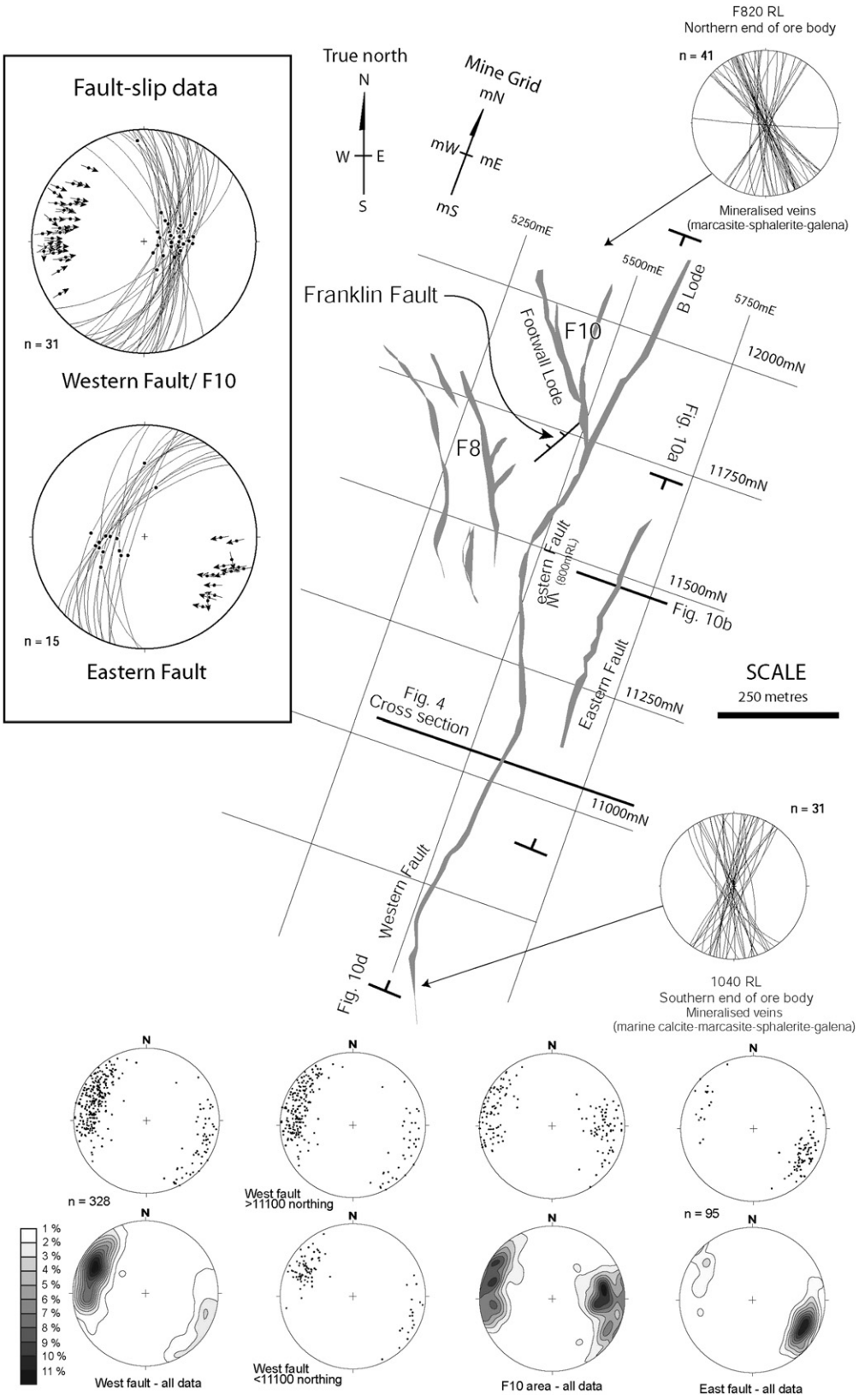

Fig. 5. Map of subsurface resource at 800 level in mine and lower hemisphere equal area spherical projections showing orientations of mineralised veins (plotted as great circles) and faults (plotted as poles and contoured with interval of 1% data per 1% net area). Inset plots show orientations of faults as great circles and slickenlines as dots; and slip linear arrows are plotted on the fault pole and show the direction of movement of the hangingwall. Section lines for Figs. 4, 10a, b, d are marked.

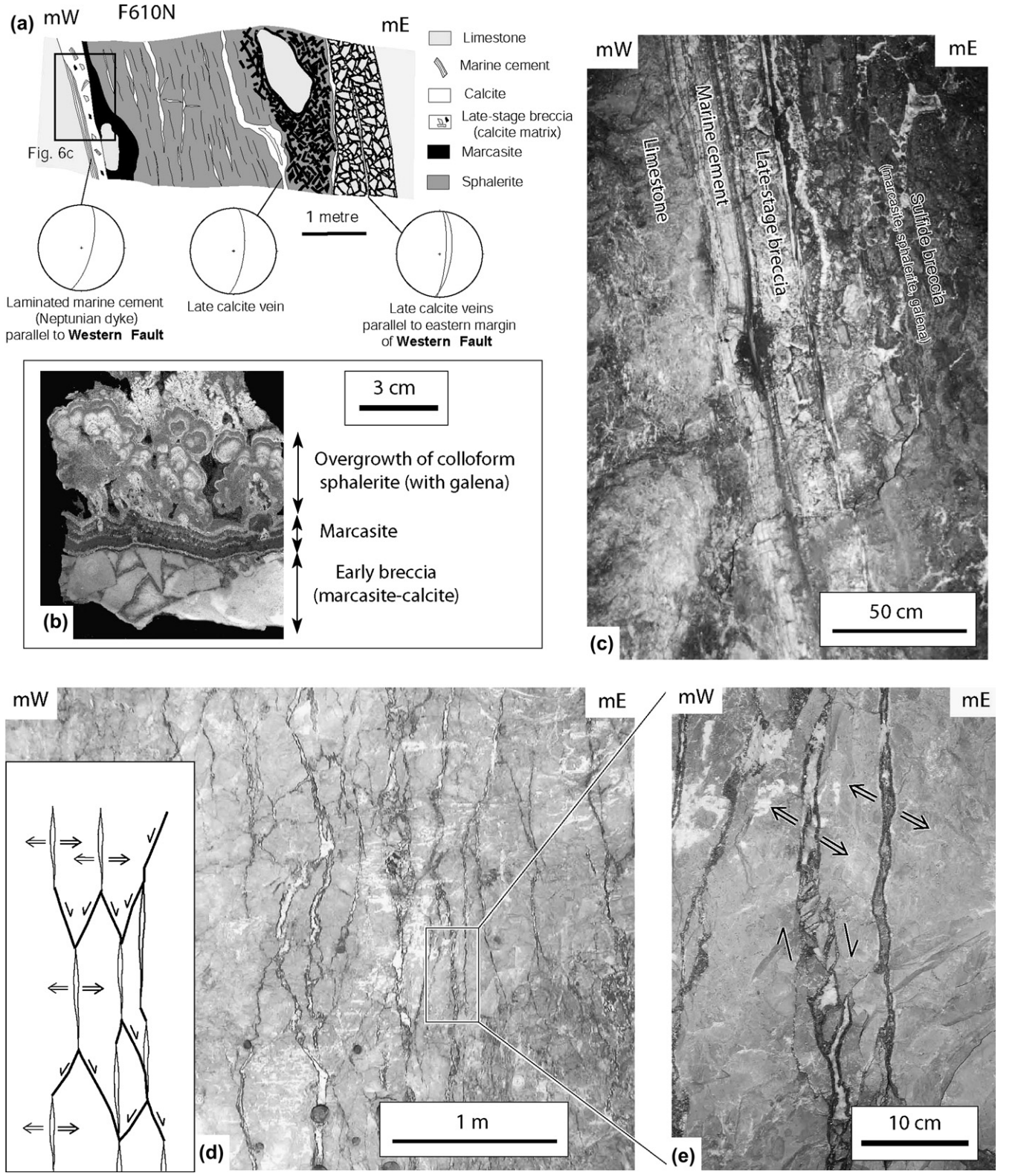

Fig. 6. (a) Cross section sketch of the Western fault on the 610 level with structural data shown on equal area spherical projections. Bands of early marine cement, marcasite-sphalerite, and late-stage breccia are sub-parallel to the fault. (b) Photograph of polished hand specimen showing early marcasite-calcite matrix breccia overgrown by later marcasite followed by colloform sphalerite (indicating growth into an open cavity). (c) Photograph of mine rib showing vein with banded early marine calcite cement, late-stage calcite matrix breccia, and earlier sulfide breccia. (d) Photograph of mine rib showing fracture mesh of mineralised steeply dipping extension and extensional shear veins adjacent to the Western fault on the 1040 level. The dark mineral on the edges of the veins is sphalerite. The white mineral is later calcite infill. (e) Detail of (d) showing *en echelon* veins linking two extensional shear veins.

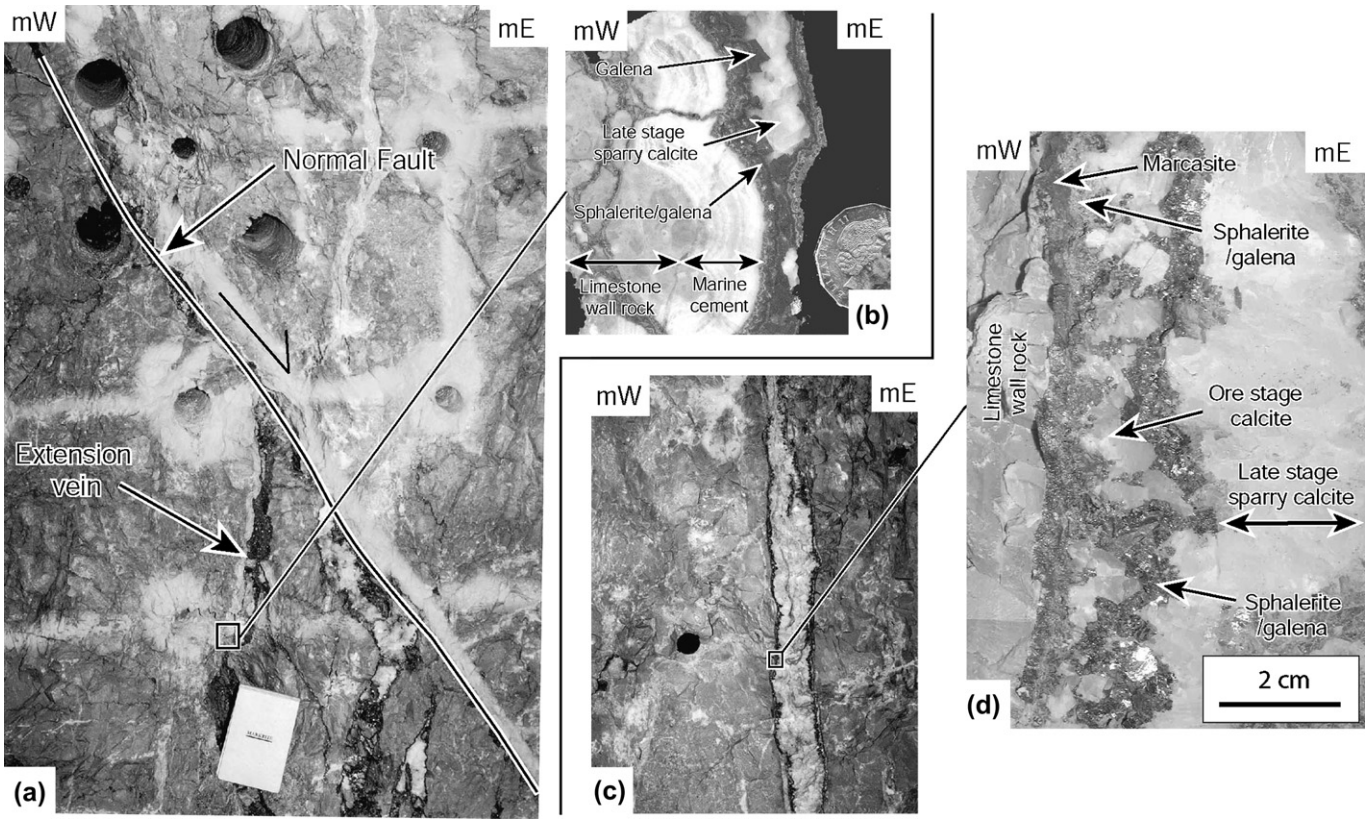

Fig. 7. Underground photographs of structural and paragenetic relations on the Western fault. (a) Normal fault with footwall extension veins on 1040 level; note that mine production paint lines are present in a grid between some drill holes and along fault; field book for scale near bottom. (b) Close-up of (a) showing vein paragenesis at relatively shallow level; early marine cement is followed by sphalerite–galena and then late-stage calcite; coin for scale (c) Steep extension vein on 820 level; vein is approximately 10 cm wide. (d) Close-up of (c) showing vein paragenesis at deeper structural levels; early to late succession is marcasite followed by sphalerite–galena, ore stage calcite, sphalerite–galena, and then late-stage sparry calcite.

were controlled by kinematics of fault movement, not by stratigraphy.

Kinematic analysis of the Western fault was complicated by the large number of intersecting and diverging faults, mostly at the northern-most portion of the Pillara mine. However, at the southern end of the Pillara mine the 3D model clearly shows extension veins in the immediate hangingwall of the Western fault (Fig. 10d). The lines of intersection of these veins with the fault surface also have a nearly horizontal rake implying this segment of the Western fault was also probably a dip-slip structure during mineralisation.

The larger scale fault-vein relationships from the Western and Eastern faults thus indicate that both faults have normal dip-slip movement vectors. This is supported by the lack of overall regional-scale lateral displacement of stratigraphic units on surface maps that preclude a major component of strike-slip movement (Fig. 4).

Some fault surfaces in the Pillara mine are strongly striated by friction grooves (slickenlines) on galena-rich fault surfaces (Fig. 9a, b). Cross-cutting relationships indicate that these slickenlines are late-stage and post-date the main Zn–Pb mineralisation. Measurements of the late-stage slickenlines indicate dominantly dip-slip movement, with fault segments (generally northeast-trending) having a component of sinistral movement. The Pillara mine also preserves sphalerite stalactites within various ore drives (Fig. 11). The long axes of these indicate post-mineralisation tilting of up to 10° to the north for some rocks (Fig. 11b); the amount of tilting within the study area is unconstrained.

4. Interpretation of structural data

4.1. The Limestone Billy Hills orthorhombic fault–fracture system

The E- and W-dipping faults in the Limestone Billy Hills region have rhombic patterns in map view, and do not conform to widely accepted Andersonian (Anderson, 1951) models of fault development that utilise Mohr–Coulomb theory. One of the key assumptions of Mohr–Coulomb theory is that the intermediate principal stress has no control on the orientation of neo-formed faults (e.g., Mandl, 2000) and the pole to any neo-formed fault always is perpendicular to σ_2 (Fig. 2b). Three-dimensional strain experiments on various rock types and analogue materials have produced orthorhombic fault geometries that do not follow Mohr–Coulomb behaviour (Oertel, 1965; Aydin and Reches, 1982; Reches and Dietrich, 1983). Orthorhombic fault geometries, which show rhombic patterns in both map and cross section views (Fig. 2c), also have been predicted by theoretical studies (Reches, 1978,

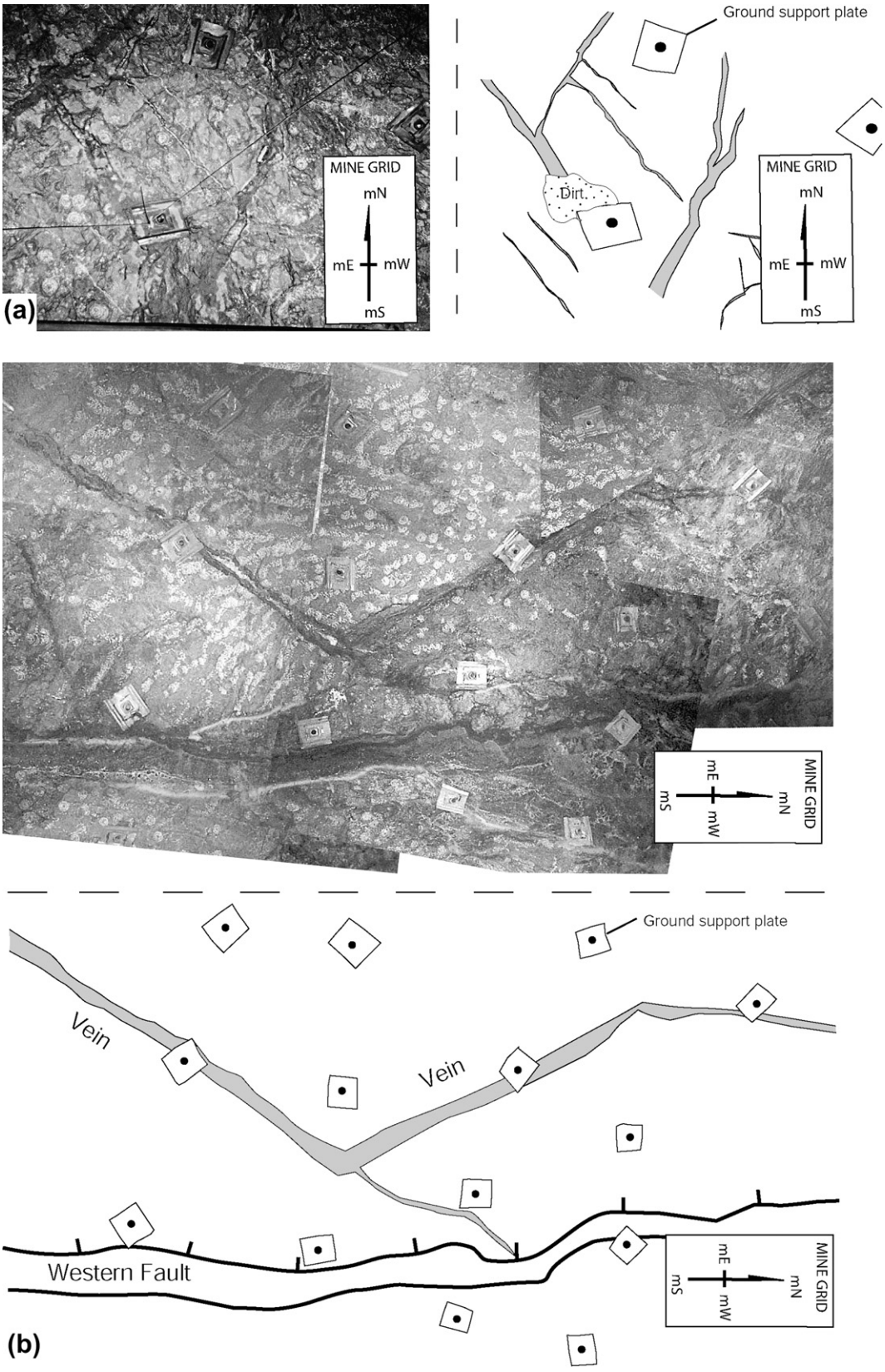

Fig. 8. Underground photographs and explanatory sketches of rhombic fracture patterns in the backs (ceilings) of underground drives. Grey is mineralised veins, white is limestone wall rock. Ground support plates are about 40 cm wide. (a) Footwall of the Western fault on 585 level. (b) Footwall of the Western fault on 875 level. Note sudden strike changes in veins.

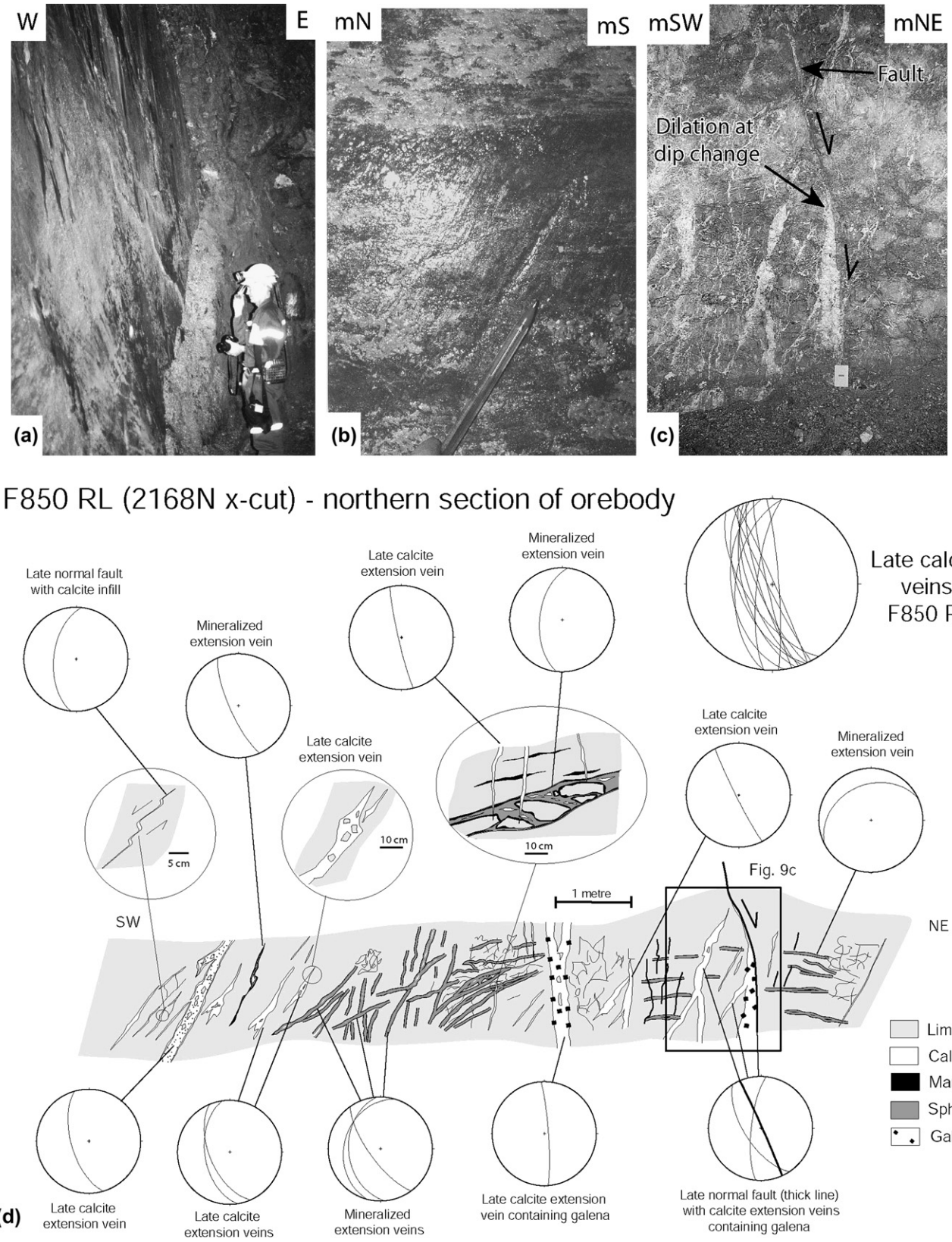

Fig. 9. Late-stage extensional structures. (a) Galena-coated fault surface. (b) Obliquely raking slickenlines defined by wear marks on galena surface (pencil for scale). (c) Late–stage normal fault associated with calcite vein at dip change in fault (field book at base for scale). (d) Section line in mine drift at 850 level showing late-stage calcite veins associated with galena and associated faults that overprint earlier mineralised structures. Lower hemisphere equal area spherical projections show structural data.

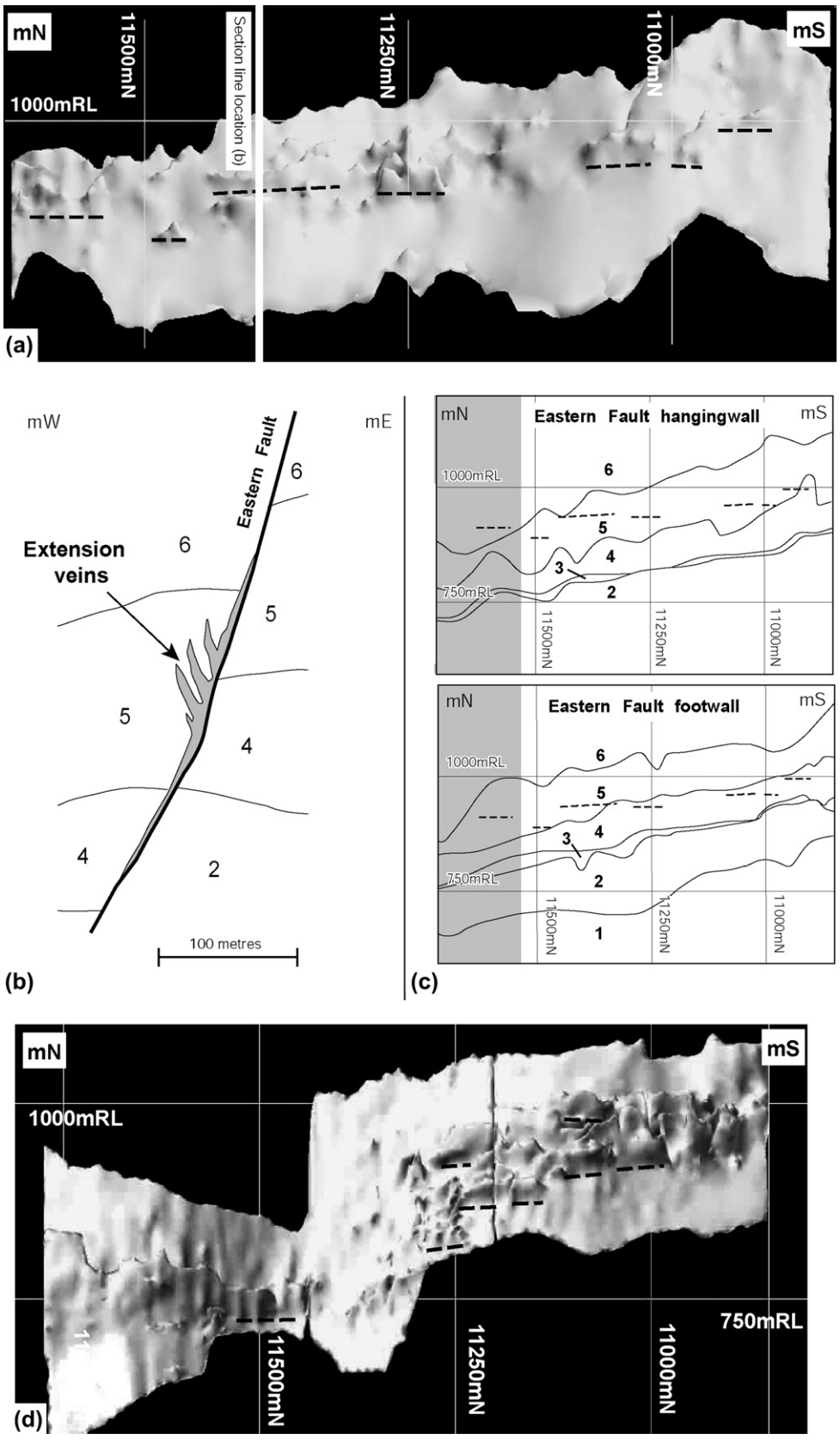

Fig. 10. (a) Portion of gOcad.™ model showing long section shaded relief view of 3% zinc equivalent volume for the Eastern fault; section line is shown on Fig. 5. Dashed lines highlight horizontal intersections between steep mineralised extension veins and the mineralised Eastern fault and are perpendicular to the slip line of the fault. (b) Cross section through the Eastern fault; section line marked in (a) and on Fig. 5. Grey shows the 3% zinc equivalence volume. Zinc equivalence is defined in the caption to Fig. 5. Note the steep extension veins in the hangingwall of the Eastern fault (these are mapped as extension veins because they do not

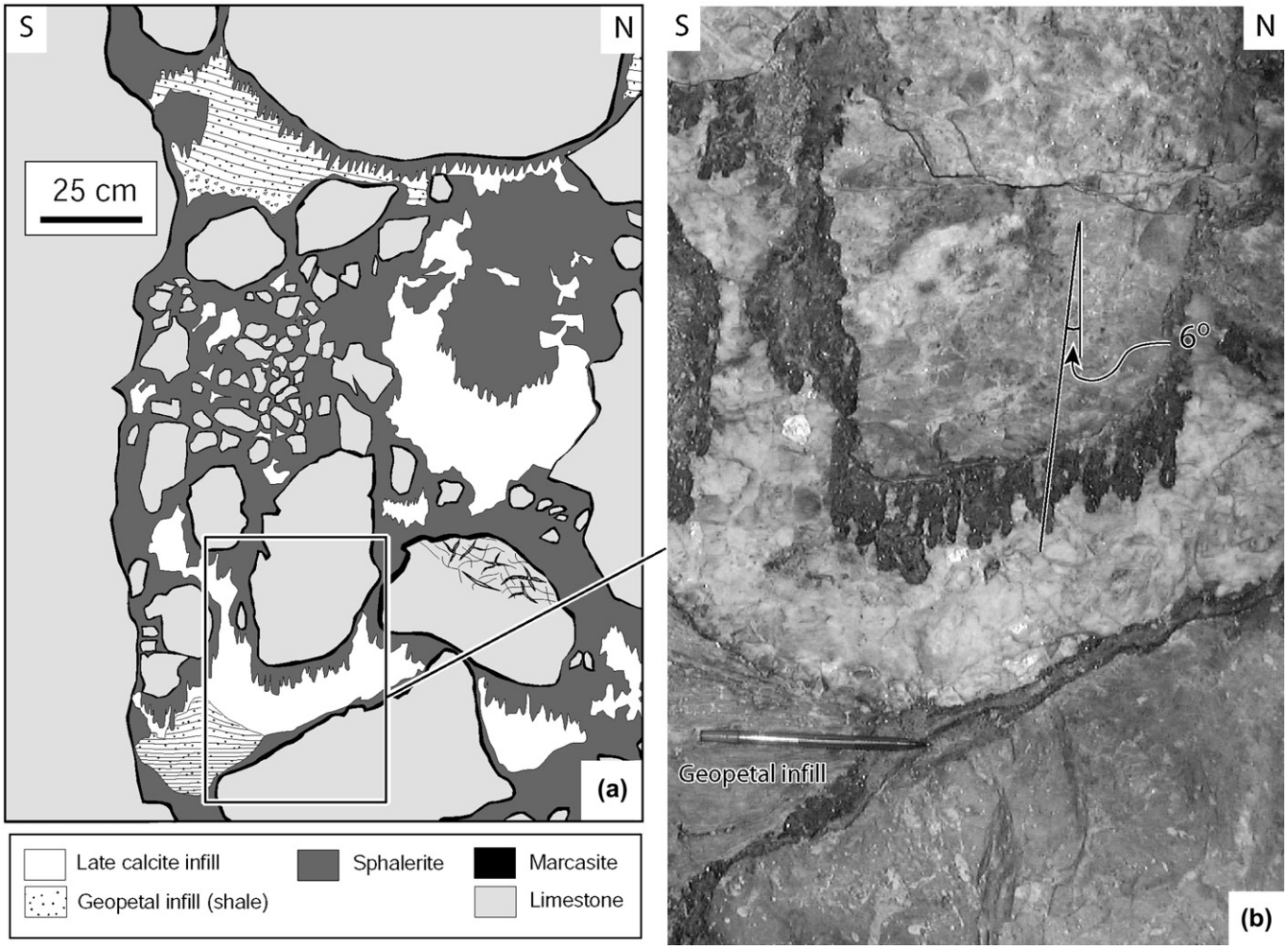

Fig. 11. (a) Sketch of mineralised breccia along the wall of an underground drive (875 RL) with sphalerite stalactites and geopetal infill. The long axes of the stalactites are inclined, indicating post-mineralisation tilting of the units. (b) Photograph of sphalerite stalactites with approximate 6° tilt; pencil for scale. The sphalerite post-dates the marine cements linked to initial fault–fracture mesh development (Fig. 7b) and indicates tilting post the development of the fault–fracture meshes.

1983). This three-dimensional strain model (Fig. 2c) has been used to interpret fault–fracture meshes in Utah, North America (Krantz, 1988a,b, 1989) and, in a failed triple junction in Africa (Oesterlen and Blenkinsop, 1994), and for fault geometries developed around a regional flexure within the Dead Sea pull apart basin in the Middle East (Sagy et al., 2003).

The faults, and the associated veins, have a geometry that is similar to the orthorhombic pattern described in the 3D fault model of Reches (1978) and Reches and Dietrich (1983) (Fig. 2b). This model argues that at least 3 (and normally 4) sets of faults are required to accommodate three-dimensional non-plane strain (Fig. 2c). The orthorhombic geometry of the normal faults and extension fractures in plan view indicate that elongation (e) was positive (extensional strain) in at least two principal directions ($e = (l'_A - l_A)/l_A$; where l'_A is the final length in direction A, and l_A is the initial length also in direction A). This strain type is equivalent to the Field 1 strain ellipsoid shape of Ramsay and Huber (1983, Fig. 4.10) that is associated with chocolate tablet boudinage and non-plane strain.

Krantz (1988a,b, 1989) studied naturally occurring faults to develop a method for determining the orientations and relative magnitudes of the principal extension (strain) axes (ϵ_1, ϵ_2, ϵ_3) associated with orthorhombic fault geometries. This method is termed the ''odd axis'' construction where the odd axis (ϵ_1 or ϵ_3) has a different elongation sign to the other two strain axes. In his method, the odd axis is constructed on an equal area spherical projection at the common intersection of great

offset the strata). (c) Long sections of the Eastern fault showing cut-off lines where stratigraphic boundaries intersect the footwall and hangingwall; dashed lines taken from (a). The unit 1 contact in the hangingwall of the Eastern fault is not shown due to uncertainty in the geometry at the intersection between the Eastern and Western faults (where this contact lies). Grey zone marks units that are close to the edge of the shelf with major along-strike variations in carbonate stratigraphy. (d) Portion of gOcad™ model showing long section shaded relief view of 3% zinc equivalent volume for the Western fault; section line shown on Fig. 5. Dashed lines highlight horizontal intersections between steep mineralised extension veins and the mineralised Western fault and are perpendicular to the slip line of the fault.

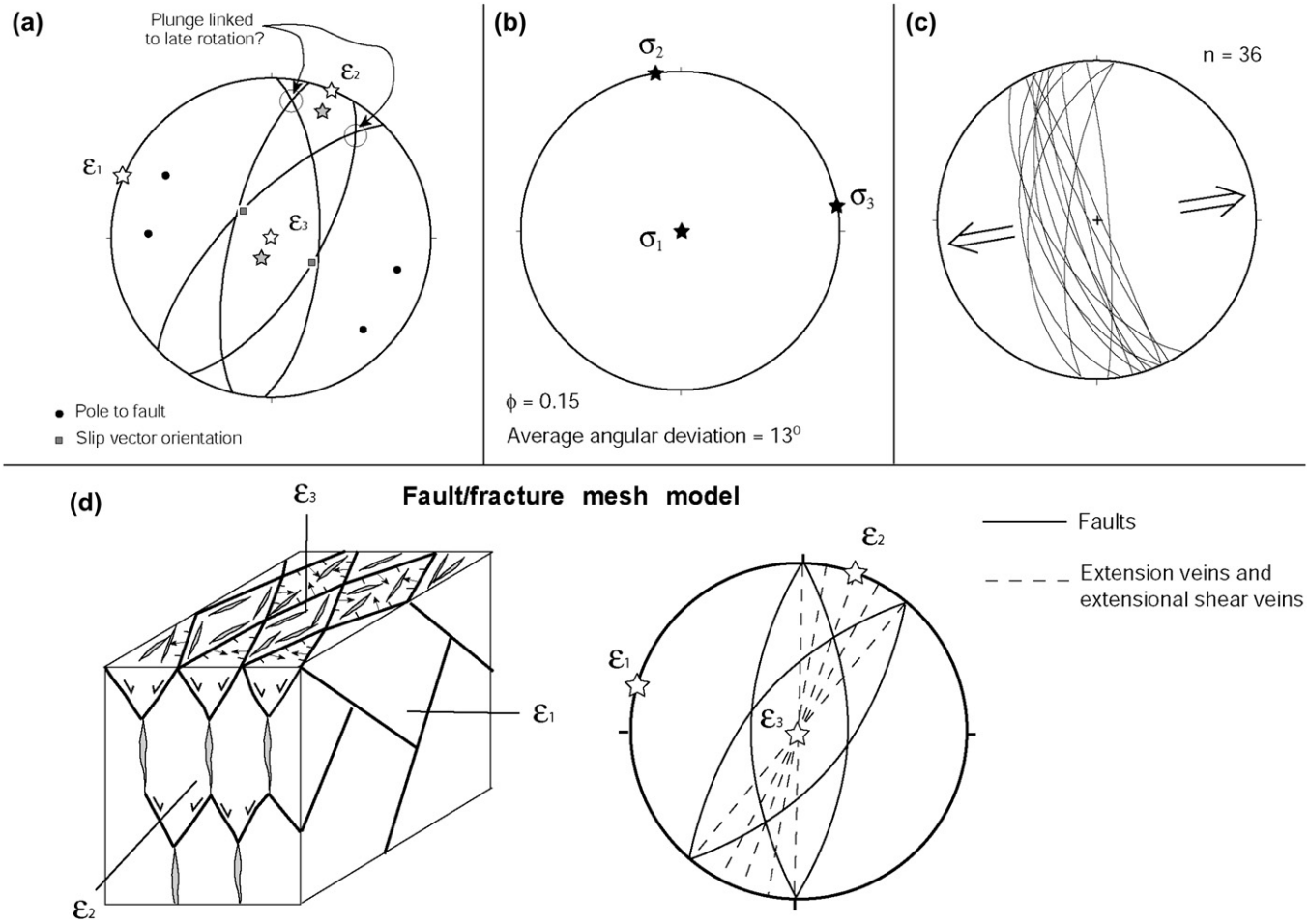

Fig. 12. Lower hemisphere equal area spherical projections (nets) showing stress and strain models and block model of fault–fracture mesh. (a) Net showing orientations of the principal finite extensions (ϵ_1, ϵ_2, ϵ_3) based an orthorhombic symmetry. Dominant fault orientations (solid lines on net) are taken from Fig. 4. Dip of east-dipping faults is approximately 65°, and west-dipping faults 70° (note slightly steeper dip of the Eastern fault on Fig. 4). Calculation is done assuming all faults are dip-slip based on analysis in Fig. 10. Note that the fault system has a slight deviation from an orthorhombic geometry that is attributed to later stage D_2 fault modification (see Fig. 13). Grey stars show predicted orientation of ϵ_2 and ϵ_3 after post-mineralisation tilting. (b) Net showing orientations of the principal stresses (σ_1, σ_2, σ_3) during late-stage normal faulting based on stress inversion modelling of fault-slickenline data in Fig. 5-inset (see text). (c) Net showing late-stage calcite veins measured on the 850 level. Arrows show approximate opening direction of veins, which is nearly parallel to the σ_3 direction obtained from stress modelling. (d) Fault–fracture mesh model that incorporates variably striking extension veins and extensional shear veins (long axis of block is N–S). Net shows predicted fault and vein orientations.

circles containing slickenline and fault pole for each fault. These great circles are the movement plane, or M-plane, of Arthaud (1969, in Aleksandrowski, 1985). The other non-ϵ_2 axis bisects the acute angle between the two clusters of great circles.

There are several complications to applying the odd axis method to the Limestone Billy Hills region. The first is that the early formed faults and fracture meshes associated with marine cement infill, and growth faulting, are overprinted by later deformation associated with distinct calcite veins and friction grooves on galena-lined fault surfaces that indicate a component of oblique-slip movement. There also appears to be block rotation with existing data suggesting post-mineralisation tilt to the north (but less than 10°; Fig. 11b). These overprints will have modified the earlier fracture mesh, but quantifying this is problematic. The odd axis method requires not just the fault orientation, but also the orientation of the slip vector. The 3D model (Fig. 10) demonstrates that the slip vector for syn-mineral movement rakes ~90° for the Eastern fault and for one segment of the Western fault (Fig. 12a). These complications have resulted in a qualitative assessment of the strain axes by assuming an orthorhombic geometry for the observed faults, and the odd axis method was not applied.

Assuming an orthorhombic symmetry for the Limestone Billy Hills region, the minimum principal strain axis (ϵ_3) is close to vertical (resulting in vertical shortening; Fig. 12a). The maximum principal strain axis (ϵ_1) is oriented shallowly towards 295°, and the intermediate principal strain axis (ϵ_2) is oriented shallowly towards 025° (Fig. 12a). The uncertainties on these estimates will be large (most likely ± 15°). The current geometry ϵ_2 suggests a slight plunge component to ϵ_2 with ϵ_3 slightly off vertical (grey stars on Fig. 12a), this may reflect late-stage rotation of the system recorded by tilted sphalerite stalactites (Fig. 11).

Stress inversion of the fault-slickenline data measured underground was done using the program SLICK.BAS in Ramsay and Lisle (2000). Whilst there is some debate over whether the results from this modelling reflect principal strain axes or principal stress axes (Twiss and Unruh, 1998), we consider the results from the modelling as orientations of the principal stress axes. In this paper we define the maximum principal stress as σ_1, the minimum principal stress as σ_3, and compressive stress has a positive sign (cf. Ramsay and Lisle, 2000). The modelling results were (Fig. 12b), $\sigma_3 = 0°/261°$, $\sigma_2 = 0°/351°$ and $\sigma_1 =$ vertical. The stress shape ratio, $(\phi = (\sigma_2 - \sigma_3)/(\sigma_1 - \sigma_3)$; Angelier, 1994) was 0.15; and the average deviation of the measured slip directions from the theoretical, recorded as a difference in rake, was 13°. The dominant opening direction (ϵ_1) of the late calcite extension veins within the Pillara mine (Fig. 9) matches the σ_3 direction obtained from the stress inversion of the fault-slickenline data (Fig. 12c).

5. Discussion and conclusions

5.1. Model for the formation of the fault–fracture mesh

Early marine cement in faults and extension veins (Figs. 6c and 7b) indicates the fault–fracture meshes developed while the system was still open to seawater prior to (and during?) the blanketing of the reefs by early Carboniferous shallow marine units. Therefore, the analysis of vein and fault structures with early marine cement constrains the fault kinematics to the Late Devonian. This inference is supported by the evidence for growth faulting in the hangingwall of the Western fault (cross section in Fig. 4). This indicates the faults are Frasnian (Late Devonian) in age (Playford, 1980; Wallace et al., 2002), and are older than the Zn–Pb mineralisation that occurred in either the latest Late Devonian, or the earliest Early Carboniferous (Famennian or Tournaisian; Christensen et al., 1995; Brannon et al., 1996). Cross-cutting relationships indicate that the measured lineations on the fault surfaces (Fig. 5) are late-stage and post-date the main Zn mineralisation, and therefore also the initial development of the fault–fracture meshes.

The rhombic fault–fracture map pattern indicates that deformation occurred in response to three-dimensional non-plane strain producing an extensional fault–fracture mesh (e.g., Fig. 6d, e) that in profile is similar to that described by Sibson (2000), but with the additional complication of being rhombic in map view (Fig. 12d). Within the Pillara mine area the strike of the veins is more variable than the strike of the faults (the faults predominantly strike northeast or north within the Limestone Billy Hills). Theoretical studies suggest that at shallow crustal levels a near-surface normal fault will splay into sub-vertical extension and extensional shear veins as the vertical stress (σ_1) magnitude approaches zero (Sibson, 1998). Offset markers are rare across the sub-vertical veins and many of the veins may actually be small displacement extensional shear veins. Some of the strike variation in the veins (Fig. 5) could reflect a combination of extensional shear veins that have strikes between faults of the dominant rhombic fault pattern and extension veins that formed perpendicular to the maximum elongation direction (ϵ_1) (Fig. 12d). Some veins also may record a local stress field in the direct hangingwall or footwall of the variably striking normal faults, i.e., the veins opened as extension fractures during slip along these faults.

Because of the variability in vein orientation we propose an initial fracture mesh (D_1) with three distinctly striking fault–fracture orientations (Fig. 13a). This matches the observed geometry of the sub-vertical veins in the mine (e.g., three different vein strikes in Fig. 8b) and implies that at a local/mine scale 6 sets of normal faults may have accommodated strain, although regionally within the Limestone Billy Hills the faults have rhombic form in map view (Fig. 3). The orthorhombic fault model of Reches (1983) requires a minimum of 4 fault sets to accommodate three-dimensional coaxial strain.

The entire system is overprinted by late normal fault movement with a minor oblique-slip component (D_2), this is inferred to have caused modification of the earlier formed orthorhombic geometry. Associated calcite veins indicate a consistent extension direction (Fig. 12c), and do not define orthorhombic patterns. The combination of oblique-slip and dip-slip slickenlines on the faults is interpreted as reflecting reactivation of the existing orthorhombic fault geometry (Fig. 13b). The slickenlines occur on mineralised fault surfaces (normally coated with galena) and constrain slip to have occurred during, or after the Zn–Pb mineralisation (<350 Ma; McManus and Wallace, 1992; Christensen et al., 1995; Brannon et al., 1996). The extension direction may have rotated counter-clockwise relative to that associated with orthorhombic faulting (Fig. 13a, b). Note that to make this comparison it needs to be assumed that either the ϵ_1 obtained from assuming orthorhombic symmetry (Fig. 12a) is parallel to σ_3, or alternatively that the σ_3 obtained from the stress inversion of fault slip-data (Fig. 12b) is parallel to ϵ_1.

5.2. Implications for basin formation and the development of transfer zones

A key problem is how to relate the development of the observed fault system within the Limestone Billy Hills area to basin-scale faults and basin development. At a regional scale ($>10 \times 10$ km), the rhombic map pattern within the Limestone Billy Hills area is not observed (Fig. 1c), indicating probable scale-dependant behaviour on the development of an orthorhombic fault geometry. The faults within the Limestone Billy Hills area (which are parallel to regional transfer zones) show evidence of growth faulting (Fig. 4), as do the faults parallel to the basin margin (e.g., the Virgin Hills fault; Dörling et al., 1996a,b). Therefore, we interpret both sets of faults to be syn-sedimentary with respect to the Devonian carbonate deposition and are interpreted to reflect strain from a single protracted deformation during basin formation.

The orthorhombic fault geometry within the Limestone Billy Hills area reflects a major component of basin parallel WNW–ESE extension and a minor component of basin-normal NNE–SSW extension within the study area. This strain pattern could be interpreted in several ways, with the scale-dependant nature

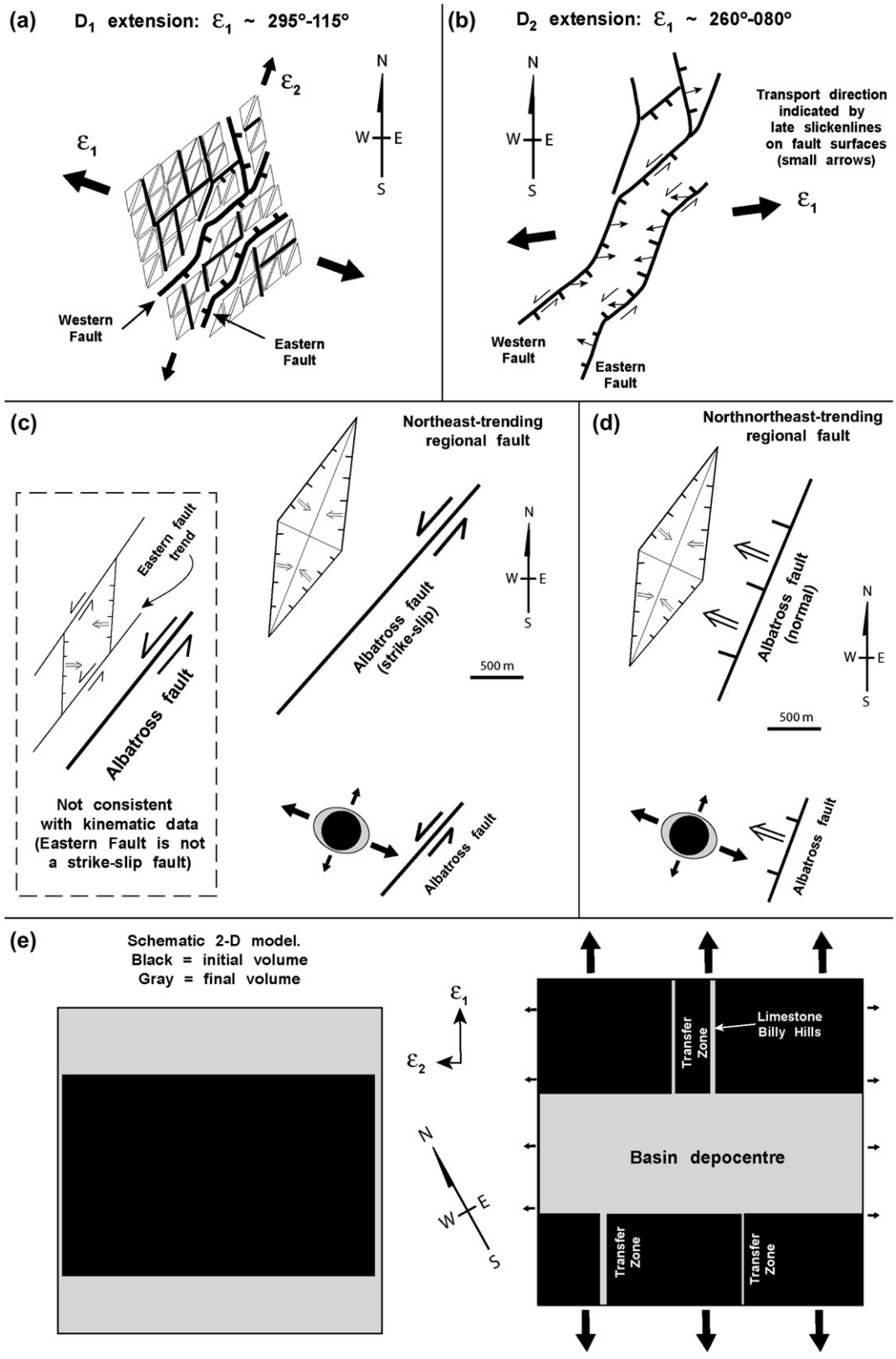

Fig. 13. Structural models for the Pillara fault–fracture mesh. (a) D_1 extension reflects non-plane strain with the formation of rhombic fault patterns; the dominant extension direction is 115°–295°. Faults are thick lines, fractures are thin lines. (b) D_2 extension caused dip-slip and oblique-slip reactivation of the earlier fracture mesh extension direction is 80°–260°. Note slightly larger map scale from (a). (c) Model with rhombic fault pattern aligned asymmetrically with respect to regional transfer zone faults; grey ellipse and arrows show stage 1 non-plane strain ellipse from (a) with black reference circle inside. (d) Preferred model with rhombic fault pattern aligned symmetrically with respect to regional transfer zone faults. (e) Simple 2D map view model for regional Devonian extensional non-plane strain; note that this diagram only depicts the regional ϵ_1 and ϵ_2 not ϵ_3 (which is vertical). Overall area change in model is highlighted by grey box

of the structural analysis being critical. The interpretation made depends on whether the orthorhombic faults, and associated extension direction, are symmetrical or asymmetrical with respect to the regional transfer zone faults (Fig. 13c,d) – both interpretations could be made from the existing geological maps. The regional faults rarely outcrop and they have variable strikes inferred from geophysical data sets that range from northeast- to north-northeast-trending (Fig. 1c).

A model of northeast-trending strike-slip faults and north-trending normal faults (inset for Fig. 13c) is not consistent with existing kinematic data. This is because there is no evidence for a substantial component of strike-slip movement on faults that are sub-parallel to the Albatross fault (e.g., the Eastern fault; Fig. 10a,b) and is reflected by the lack of consistent strike separation across grabens in the Limestone Billy Hills (Fig. 3).

If the local faults are asymmetrical about the regional transfer zone faults (such as the Albatross fault; Fig. 1c) then strain partitioning occurred during development of the LBHTZ. The Limestone Billy Hills area represents a region of extensional non-plane strain between major strike-slip transfer faults (Fig. 13c). In this model, the zones between the transfer faults had a maximum extension direction that was not perpendicular to the strike of the adjacent transfer fault (Fig. 13c). The lack of observable offset of the basin bounding faults by the transfer faults (i.e., Virgin Hills Fault and Albatross Fault; Fig. 3c) indicates the net amount of strike-slip movement must have been small enough not to be observed at a regional scale.

We argue that at a regional scale the rhombic fault map pattern (Fig. 3) is closer to being symmetrical about the regional NNE-trending faults, with no major asymmetry to the system (Fig. 13d). There is no change in half graben polarity, nor is their evidence for a major step in the overall basin margin along strike from the LBHTZ (Fig. 1c), and therefore no need for strike-slip transfer faults to have developed within this segment of the basin during rifting. Our observations from the Limestone Billy Hills area, and the regional fault geometries, are more compatible with the overlapping synthetic transfer zone having initially developed (D_1; Fig. 13a) from a component of extension sub-parallel to the basin margin, rather than as strike-slip or oblique-slip structures (Fig. 13e). A subsequent D_2 transtensional overprint of the system (Fig. 13b), evidenced by slickenlines and late calcite veins, modified the fault–fracture mesh.

Strain associated with the development of the normal faults along the Lennard shelf is inferred to have a geometry that lies between axially symmetric extension, such as that represented by a ridge-ridge-ridge triple junction, and plane strain such as that represented by ‘‘classic’’ normal faults separated by strike-slip transfer faults that are analogous to transform faults at mid-ocean spreading ridges. The normal faults accommodated a major *regional* component of NNE–SSW extension (major basin bounding faults) and a much smaller component of WNW–ESE extension. Some of the transfer zones, such as the LBHTZ, are inferred to have developed in response to the component of WNW–ESE extension (Fig. 13e). The transfer zones reflect localisation of that component of the regional strain ellipsoid, and represent one type of synthetic overlapping transfer zone. This model also does not preclude some component of strike-slip movement associated with the transfer zones. The late-stage slickenlines and extension vein data from the Pillara mine indicate it is possible that once the transfer zones develop they may then become transtensional in nature during continuing extension and basin development.

An alternate interpretation is that the LBHTZ is a breached relay ramp (Childs et al., 1995), with the WNW–ESE extension recorded by the faults within the LBHTZ being a local feature linked to gravitationally driven down-dip extension on reoriented bedding surfaces that defined an earlier relay ramp (Fig. 2a). The strike and dip of a relay ramp is related to the amount of overlap between the two normal faults linked by the relay ramp, and also the displacement gradients between the normal faults (Peacock and Sanderson, 1991). Some relay-ramps trend at a right angle to the dominant normal faults (e.g., Peacock and Sanderson, 1991), however, most breached relay-ramps (Childs et al., 1995) are disrupted by faults that are not at a right angle to the main basin parallel normal faults, as occurs on the Lennard Shelf.

We infer that the WNW–ESE extension was dominant within the LBHTZ, but there was still a component of regional NNE–SSW extension resulting in the development of the observed orthorhombic fault geometries (Figs. 3, 4). There is no clear reference to orthorhombic faults within synthetic overlapping transfer zones in the literature, however, complex polygonal fault-bounded blocks (Fig. 2a) have been previously documented in other rift systems within overlapping synthetic transfer zones, e.g., the Kenya rift highlighted in Fig. 7 of Morley et al. (1990). Irrespective of whether the observed WNW–ESE extension in the LBHTZ is a local or regional phenomena, synthetic overlapping transfer zones are inferred to be key regions where orthorhombic fault geometries could develop.

Transfer zones are generally transverse or oblique zones along rifts or extensional terranes which bound regions of opposite fault dip and/or different structural styles, or across which localized brittle extensional strain is offset. The results of this study suggest that transfer zones could also form as part of a non-plane strain field in which a component of extension orthogonal to the regional maximum finite extension direction was associated with basin formation.

Acknowledgments

The 3D model was produced using gOcad™ by Thong Nghuyh at the Australian Crustal Research Centre, School of Geoscience, Monash University. Western Metals Pty. Ltd., is

with black box marking initially volume. Area change is accommodated by the formation of basin parallel faults (e.g., Pinnacle fault, Virgin Hills fault; Fig. 1c) that reflect the dominant NNE–SSW extension direction (ϵ_1) these produce the main basin depocentre. The transfer zones form as a result of a smaller component of WNW–ESE extension (ϵ_2); the Limestone Billy Hills area and Pillara mine are in the northern zone. Some accommodation structures may subsequently develop strike-slip components.

thanked for financial and logistical support. This work was funded by NSF Grant EAR-0073763 with data input from a regional BHP minerals division mapping program done in the early 1980s that first delineated the orthorhombic fault geometries (W.D.M. Hall) and work done by Western Metals Pty Ltd Geologists (P. Muccilli). Tom Blenkinsop is thanked for providing a reprint of some insightful structural work in the Zambezi and Luangwa Rift Zones, Southern Africa. An anonymous reviewer and detailed constructive reviews by Richard Jones and John J. Walsh substantially improved the manuscript.

References

Aleksandrowski, P., 1985. Graphical determination of principal stress directions for slickenside lineation populations: an attempt to modify Arthaud's method. Journal of Structural Geology 7, 73–82.

Anderson, E.M., 1951. The Dynamics of Faulting, second ed. Oliver and Boyd, Edinburgh.

Angelier, J., 1994. Fault slip analysis and palaeostress reconstruction. In: Hancock, P.L. (Ed.), Continental Deformation. Pergamon, Oxford, pp. 53–100.

Arthaud, F., 1969. Méthode de determination graphique des directions de raccourcissement, d'allongement et intermédiaire d'une papulation de failles. Bulletin Societé géologique de France 7, 729–737.

Aydin, A., Reches, Z., 1982. Number and orientation of fault sets in the field and in experiments. Geology 10, 107–112.

Bally, A.W., 1981. Atlantic type margins. In: Geology of Passive Continental Margins: History, Structure and Sedimentologic record. AAPG Education Course Notes Series, vol. 19, pp. 1–48.

Bosworth, W., 1985. Geometry of propagating rifts. Nature 316, 625–627.

Brannon, J.C., Cole, S.C., Podosek, F.A., Ragan, V.M., Coveney, R.M., Wallace, M.W., Bradley, A.J., 1996. Th–Pb and U–Pb dating of ore-stage calcite and Palaeozoic fluid flow. Science 71, 491–493.

Brown, S.A., Bosercio, I.M., Jackson, K.S., Spence, K.W., 1984. The geological evolution of the Canning Basin – implications for petroleum exploration. In: Purcell, P.G. (Ed.), The Canning Basin, W.A: Proceedings of the Geological Society of Australia/Petroleum Exploration Society of Australia Symposium, Perth, pp. 85–96.

Childs, C., Watterson, J., Walsh, J.J., 1995. Fault overlap zones within developing normal fault systems. Journal of the Geological Society, London 152, 535–549.

Christensen, J.N., Halliday, A.N., Vearncombe, J.R., Kesler, S.E., 1995. Testing models of large-scale crustal fluid flow using direct dating of sulfides; Rb-Sr evidence for early dewatering and formation of Mississippi Valley-type deposits, Canning Basin, Australia. Economic Geology 90, 877–884.

Dörling, S.L., Dentith, M.C., Groves, D.I., Vearncombe, J.R., 1996a. Mississippi Valley-type deposits of the of the Southeastern Lennard Shelf: an example of the interplay of extensional deformation, sedimentation and mineralization. In: Sangster, D.F. (Ed.), Carbonate-hosted lead-zinc deposits. Society of Economic Geologists, Special Publications, vol. 4, 96–111.

Dörling, S.L., Dentith, M.C., Groves, D.I., Playford, P.E., Vearncombe, J.R., Muhling, P., Windrum, D., 1996b. Heterogeneous brittle deformation in the Devonian carbonate rocks of the Pillara Range, Canning Basin: implications for the structural evolution of the Lennard Shelf. Australian Journal of Earth Sciences 43, 15–29.

Faulds, J.E., Varga, R.J., 1998. The role of accommodation zones and transfer zones in the regional segmentation of extended terranes. In: Faulds, J.E., Stewart, J.H. (Eds.), Accommodation Zones and Transfer Zones: The Regional Segmentation of the Basin and Range Province. Geological Society of America, Special Paper vol. 323, 1–46.

George, A.D., Playford, P.E., Powell, C.McA., Tornatora, P.M., 1997. Lithofacies and sequence development on an Upper Devonian mixed carbonate-siliciclastic fore-reef slope, Canning Basin, Western Australia. Sedimentology 44, 843–867.

Gibbs, A.D., 1983. Balanced section constructions from seismic sections in areas of extensional tectonics. Journal of Structural Geology 5, 153–160.

Gibbs, A.D., 1984. Structural evolution of extensional basin margins. Journal of the Geological Society 141, 609–620.

gOcad website. http://gocad.ensg.inpl-nancy.fr.

Guiraud, R., Martin, J.C., 1992. Early Cretaceous rifts of Western and Central Africa. Tectonophysics 213, 153–168.

Hall, W.D.M., 1984. The stratigraphic and structural development of the Giventian–Frasnian reef complex, Limestone Billy Hills, Western Pillara Range, WA. In: Purcell, P.G. (Ed.), The Canning Basin, WA: Proceedings of the Geological Society of Australia/Petroleum Exploration Society of Australia Symposium, Perth, pp. 215–222.

Krantz, R.W., 1988a. Multiple fault sets and three-dimensional strain: theory and application. Journal of Structural Geology 10, 225–237.

Krantz, R.W., 1988b. Orthorhombic fault patterns: the odd axis model and slip vector orientations. Tectonics 8, 483–495.

Lister, G.S., Etheridge, M.A., Symonds, P.A., 1986. Detachment faulting and the formation of passive continental margins. Geology 14, 246–250.

Lister, G.S., Etheridge, M.A., Symonds, P.A., 1991. Detachment models for the formation of passive continental margins. Tectonics 10, 1038–1064.

Mandl, G., 2000. Faulting in Brittle Rocks: An Introduction to the Mechanics of Tectonic Faults. Springer-Verlag, New York, 434 pp.

McClay, K.R., Dooley, T., Whitehouse, P., Mills, M., 2002. 4D evolution of rift systems: insights from scaled physical models. American Association of Petroleum Geologists Bulletin 86, 935–959.

McManus, A., Wallace, M.W., 1992. Age of Mississippi-type sulfides determined using cathodoluminescence cement stratigraphy, Lennard Shelf, Canning Basin, Western Australia. Economic Geology 87, 189–193.

Middleton, M.F., 1990. Canning basin: Western Australia. Geological Survey Memoir 3, 456.

Miller, J.McL., Norvick, M.S., Wilson, C.J.L., 2002. Basement controls on rifting and the associated formation of ocean transform faults – cretaceous continental extension of the southern margin of Australia. Tectonophysics 359, 131–155.

Miller, J.McL., Wilson, C.J.L., 2004. Application of structural analysis to faults associated with a heterogeneous stress history: the reconstruction of a dismembered gold deposit, Stawell, western Lachlan Fold Belt, Southeastern Australia. Journal of Structural Geology 26, 1231–1256.

Morley, C.K., 1994. Structural geology of rifts. In: Lambiase, J.J. (Ed.), Hydrocarbon habitat in rift basins. Geological Society, Special Publication, vol. 80, pp. 75–102.

Morley, C.K., Nelson, R.A., Patton, T.L., Munn, S.G., 1990. Transfer zones in the East African rift system and their relevance to hydrocarbon exploration in rifts. American Association of Petroleum Geologists Bulletin 74, 1234–1253.

Moustafa, A.R., 1997. Controls on the development and evolution of transfer zones: the influence of basement structure and sedimentary thickness in the Suez rift and Red Sea. Journal of Structural Geology 19, 755–768.

Murphy, G.C., 1990. Lennard Shelf lead-zinc deposits. In: Australasian Institute of Mining and Metallurgy Monograph, vol. 14. pp.1103–1109.

Oertel, G., 1965. The mechanism of faulting in clay experiments. Tectonophysics 2, 343–393.

Oesterlen, P.M., Blenkinsop, T.G., 1994. Extension directions and strain near the failed triple junction of the Zambezi and Luangwa Rift Zones, southern Africa. Journal of African Sciences 18, 175–180.

Peacock, D.C.P., Sanderson, D.J., 1991. Displacements, segment linkage and relay ramps in normal fault zones. Journal of Structural Geology 13, 721–733.

Peacock, D.C.P., Knipe, R.J., Sanderson, D.J., 2000. Glossary of normal faults. Journal of Structural Geology 22, 291–305.

Playford, P.E., 1980. Devonian "Great Barrier Reef" of Canning Basin, Western Australia. American Association of Petroleum Geologists Bulletin 64, 814–840.

Playford, P.E., Wallace, M.W., 2001. Exhalative mineralization in Devonian reef complexes of the Canning Basin, Western Australia. Economic Geology 96, 1595–1610.

Ramsay, J.G., Huber, M.I., 1983. The techniques of modern structural geology. In: Strain Analysis, vol. 1. Academic Press, London.

Ramsay, J.G., Lisle, R., 2000. The techniques of modern structural geology. In: Applications of Continuum Mechanics in Structural Geology, vol. 3. Academic Press, San Diego.

Reches, Z., 1978. Analysis of faulting in a three-dimensional strain field. Tectonophysics 47, 109–129.

Reches, Z., 1983. Faulting of rocks in three-dimensional strain fields. II. Theoretical analysis. Tectonophysics 95, 133–156.

Reches, Z., Dietrich, J.H., 1983. Faulting of rocks in three-dimensional strain fields. I. Failure of rocks in polyaxial, servocontrolled experiments. Tectonophysics 95, 111–132.

Robert, F., Poulsen, K.H., 2001. Vein formation and deformation in greenstone gold deposits. Society of Economic Geologists Reviews 14, 111–155.

Rosendahl, B.R., Reynolds, D., Lorber, P., Burgess, C., McGill, J., Scott, D., Lambiase, J., Derksen, S., 1986. Structural expression of rifting: lessons from Lake Tanganyika. In: Frostick, L.E., et al. (Eds.), Sedimentation in the East African rifts. Geological Society, Special Publication, vol. 25, pp. 29–43.

Sagy, A., Reches, Z., Agnon, A., 2003. Hierarchic three-dimentional structure and slip partitioning in the western Dead Sea pull-apart. Tectonics 22 (1), 4-1–4-17.

Sibson, R.H., 1998. Brittle failure mode plots for compressional and extensional tectonic regimes. Journal of Structural Geology 20, 655–660.

Sibson, R.H., 2000. Fluid involvement in normal faulting. Journal of Geodynamics 29, 469–499.

Twiss, R.J., Unruh, J.R., 1998. Analysis of fault slip inversions: do they constrain stress or strain rate? Journal of Geophysical Research 103, 12,205–12,222.

Vearncombe, J.R., Dentith, M., Dorling, S., Reed, A., Cooper, R., Hart, J., Muhling, P., Windrum, D., Woad, G., 1995. Regional- and prospect-scale fault controls on Mississippi Valley-type Zn–Pb mineralization at Blendevale, Canning Basin, Western Australia. Economic Geology 90, 181–186.

Vearncombe, J.R., Chisnall, A.W., Dentith, M.C., Dorling, S.L., Rayner, M.J., Holyland, P.W., 1996. Structural controls on Mississippi Valley-type mineralization, the southeastern Lennard Shelf, Western Australia. In: Sangster, D.F. (Ed.), Carbonate-hosted lead–zinc deposits. Society of Economic Geologists, Special Publication, vol. 4, pp. 74–95.

Wallace, M.W., Middleton, H.A., Johns, B., Marshallsea, S., 2002. Hydrocarbons and Mississippi Valley-type sulfides in the Devonian reef complexes of the eastern Lennard Shelf, Canning Basin, Western Australia. In: Keep, M., Moss, S.J. (Eds.), The Sedimentary Basins of Western Australia 3: Proceedings of the Petroleum Exploration Society of Australia Symposium, Perth, WA, pp. 795–815.

Walsh, J.J., Watterson, J., 1991. Geometric and kinematic coherence and scale effects in normal fault systems. In: Roberts, A.M., Yielding, G., Freeman, B. (Eds.), The Geometry of Normal Faults. Geological Society, London, Special Publications, vol. 56, pp. 193–203.